

**Supporting Information for**

**The July-December 2022 earthquake sequence in the southeastern Fars arc of Zagros mountains, Iran**

**Metz, M.<sup>1,2</sup>, Asayesh, B. M.<sup>1,2</sup>, Aref, M. M.<sup>1</sup>, Jamalreyhani, M.<sup>2,3</sup>, Büyükpınar, P.<sup>2</sup>, Dahm, T<sup>1,2</sup>**

**Institute of Geosciences, University of Potsdam, Potsdam, Germany; GFZ German Research Centre for Geosciences, Potsdam, Germany; Institute of Geophysics, University of Tehran, Tehran, Iran**

**Contents of this file**

- Figure S1:** Waveform fits from full MT inversion for earthquake A1.
  - Figure S2:** Waveform fits from full MT inversion for earthquake A2.
  - Figure S3:** Waveform fits from full MT inversion for earthquake A3.
  - Figure S4:** Waveform fits from full MT inversion for earthquake B1.
  - Figure S5:** Waveform fits from full MT inversion for earthquake B2.
  - Figure S6:** Waveform fits from full MT inversion for earthquake C1.
  - Figure S7:** Waveform fits from single source PDR inversion for earthquake A1.
  - Figure S8:** Waveform fits from single source PDR inversion for earthquake A2.
  - Figure S9:** Waveform fits from single source PDR inversion for earthquake A3.
  - Figure S10:** Waveform fits from joint 3 double couple source inversion of earthquakes A1, A2 and A3 using satellite deformation and seismic data.
  - Figure S11:** Waveform fits from joint 3 PDR inversion of earthquakes A1, A2 and A3 using satellite deformation and seismic data.
  - Figure S12:** Waveform fits for focal depth estimation with abedeto for earthquake A1.
  - Figure S13:** Waveform fits for focal depth estimation with abedeto for earthquake A2.
  - Figure S14:** Waveform fits for focal depth estimation with abedeto for earthquake A3.
  - Figure S15:** Waveform fits for focal depth estimation with abedeto for earthquake B1.
  - Figure S16:** Waveform fits for focal depth estimation with abedeto for earthquake B2.
  - Figure S17:** Waveform fits for focal depth estimation with abedeto for earthquake C1.
  - Figure S18:** Network locations of all seismic networks used for abedeto focal depth estimation..
  - Figure S19:** Map and profile plot of the relocated aftershocks and the location uncertainties.
- Table S3:** Double couple (DC) MT solutions for the earthquakes A1-A3 from a joint 3 DC source inversion using seismic and satellite deformation data.
- Table S6:** Abedeto results including the used arrays and the derived focal depths for all mainshocks.

## **Additional Supporting Information (Files uploaded separately)**

**File Table\_S1.pdf:** Full MT solutions for the seven earthquakes A1-A3, B1, B2 and C1 derived from seismic data.

**File Table\_S2.pdf:** Deviatoric MT solutions for the seven earthquakes A1-A3, B1, B2 and C1 derived from seismic data.

**File Table\_S4.pdf:** Results for individual finite fault inversions using seismic data.

**File Table\_S5.pdf:** Finite fault solutions for the earthquakes A1-A3 from a joint 3 PDR inversion using seismic and InSAR data.

**File Table\_S7.pdf:** Aftershocks of the IRSC catalog including uncertainties after relocation using the GrowClust3D.jl algorithm.

## **Introduction**

We provide waveform fits obtained from the different full CMT and PDR finite fault inversions shown and discussed in the main text (Fig. S1–S11). They highlight the number of records available and their fit with respect to the different inversion approaches and the different earthquakes. Complementing that mean model parameters and their standard deviations are provided for deviatoric MT inversions (file Table\_S1), full MT inversions (file Table\_S2) and joint 3 double couple source inversion of sequence A (Tab.S3).

Both single source PDR solutions (file Table\_S4) as well as the joint 3 PDR inversion results (file Table\_S5) are given as well. In this regard we also yield PDR solutions for the less preferred nodal plane (file Table\_S4).

Complementing on the mainshock inversions focal depth estimations based on teleseismic P-wave depth phases are shown (Fig. S12–S17). A map of the used arrays is given in Figure S18. Both, used seismic arrays, and the focal depth estimates, are summarized in Table S6.

Besides there is also some more detailed information on the aftershock relocation. In this regard we have displayed uncertainties of the relocated catalog (Fig. S19). The supplemental file Table\_S7 provides the relocated catalog along with all uncertainties.

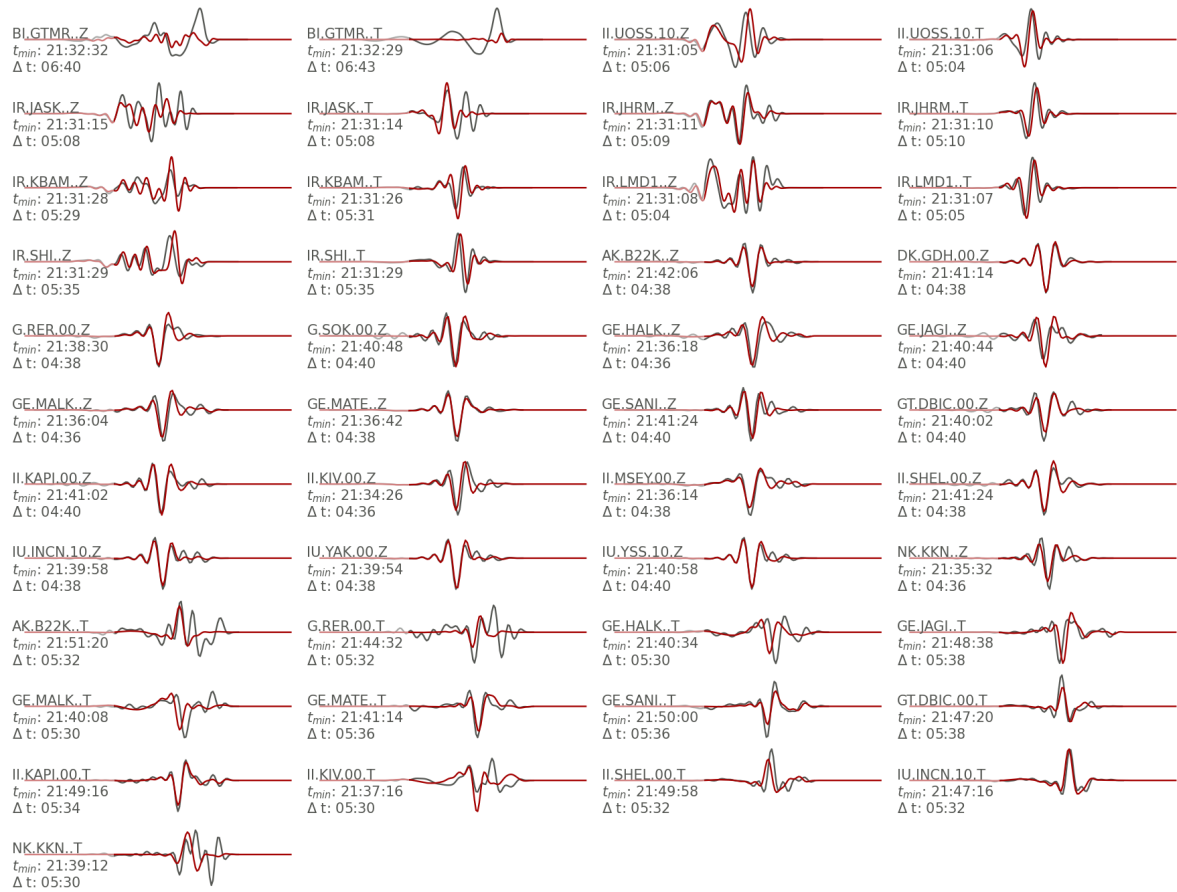


**Figure S1.** Waveform fits of the mean model (red) and observed data (black) from full MT inversion of earthquake A1. Channel information, start time of each trace and length of the given traces are given left of each trace.

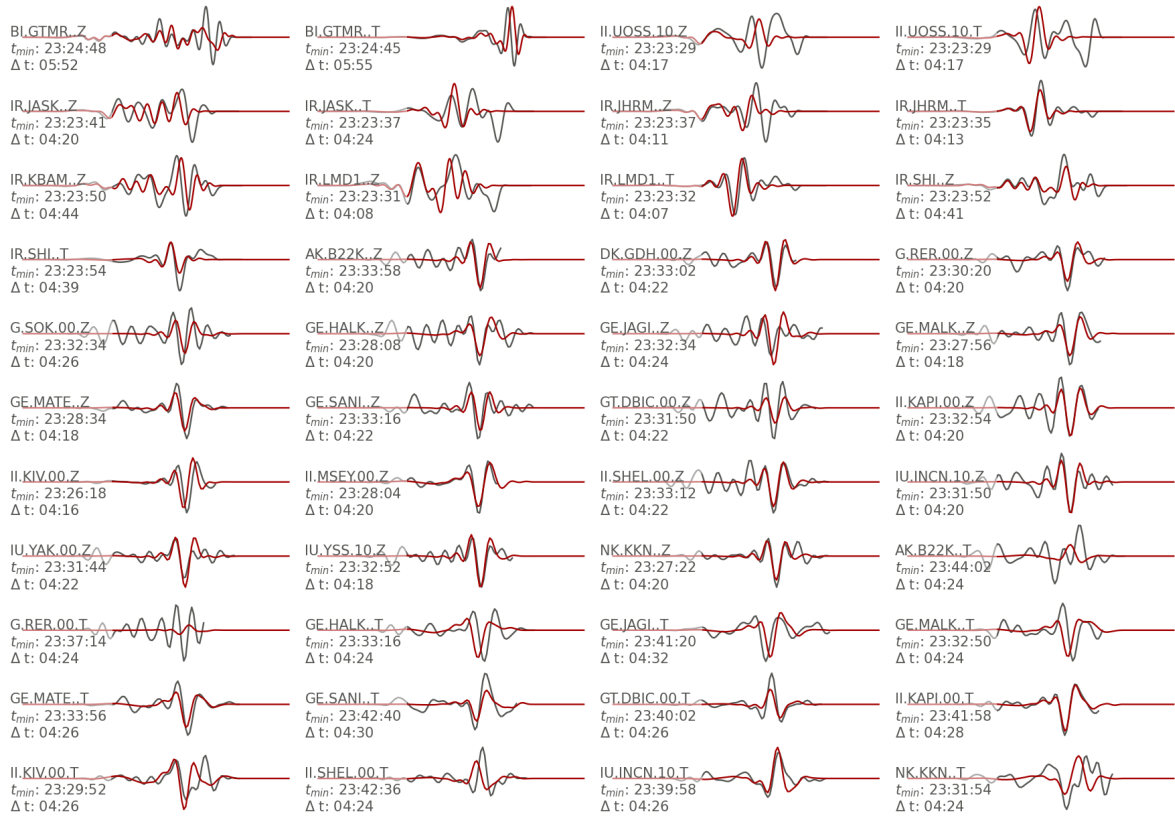


**Figure S2.** Waveform fits of the mean model (red) and observed data (black) from full MT inversion of earthquake A2. Channel information, start time of each trace and length of the given traces are given left of each trace.

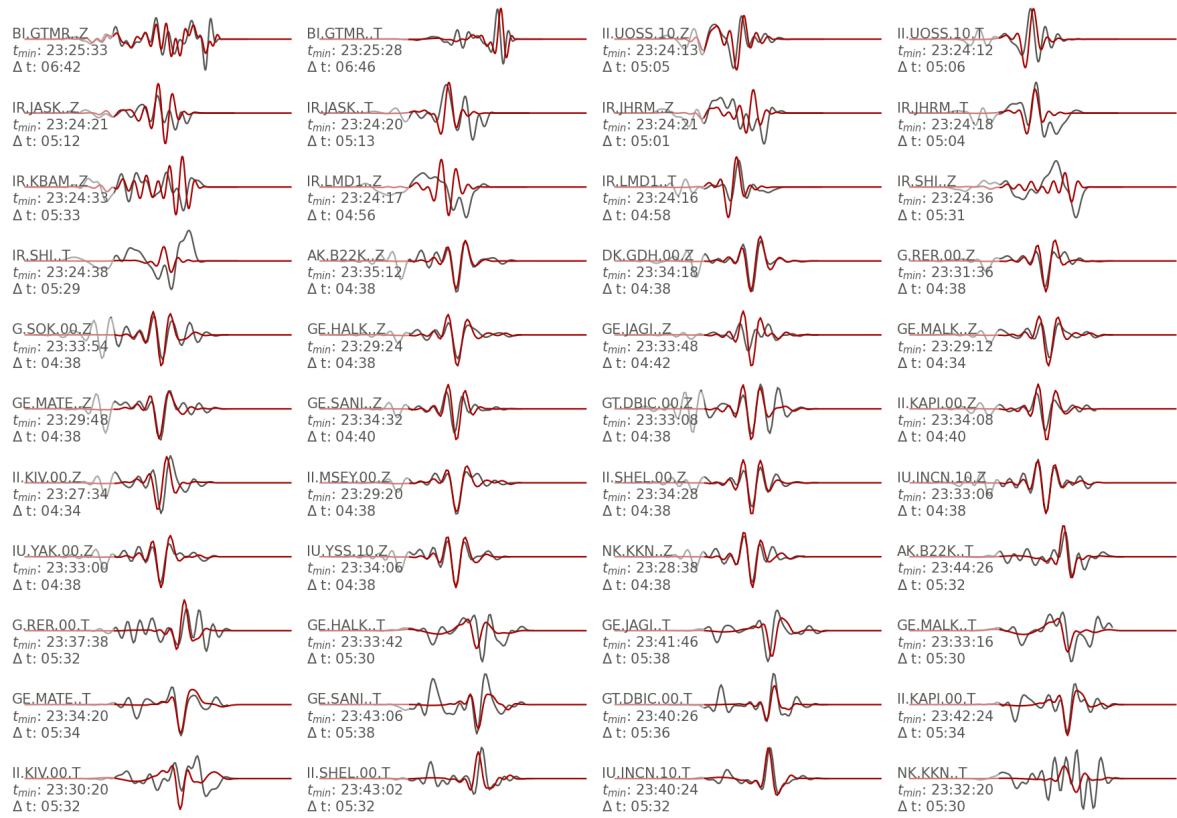


**Figure S3.** Waveform fits of the mean model (red) and observed data (black) from full MT inversion of earthquake A3. Channel information, start time of each trace and length of the given traces are given left of each trace.

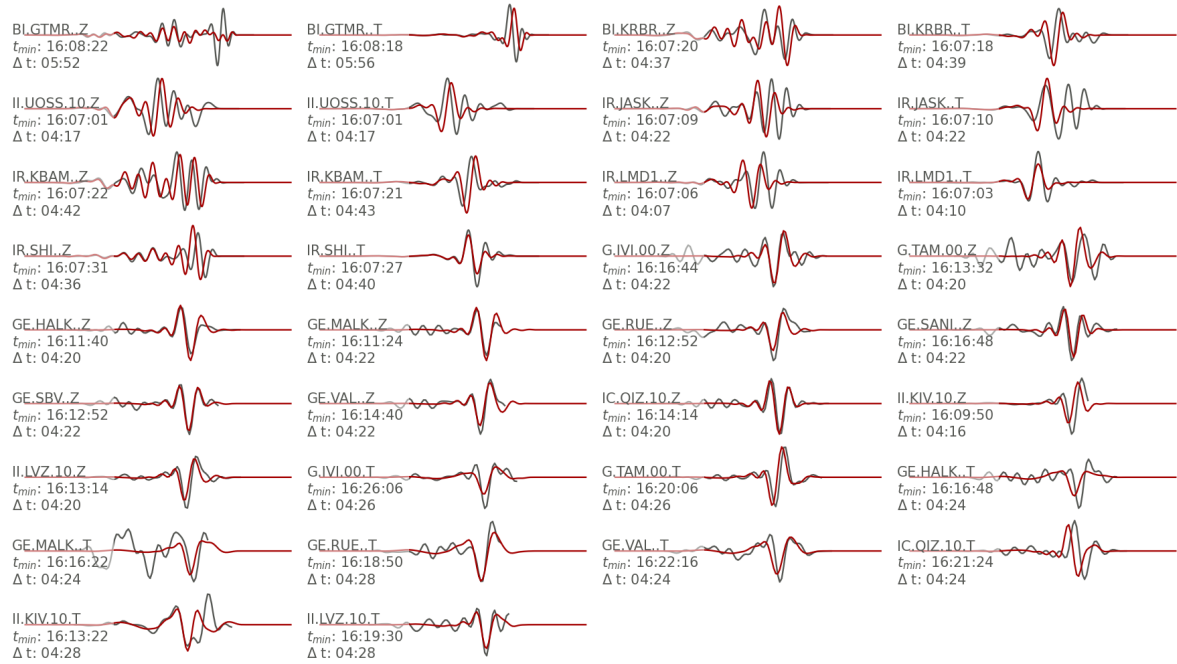


**Figure S4.** Waveform fits of the mean model (red) and observed data (black) from full MT inversion of earthquake B1. Channel information, start time of each trace and length of the given traces are given left of each trace.

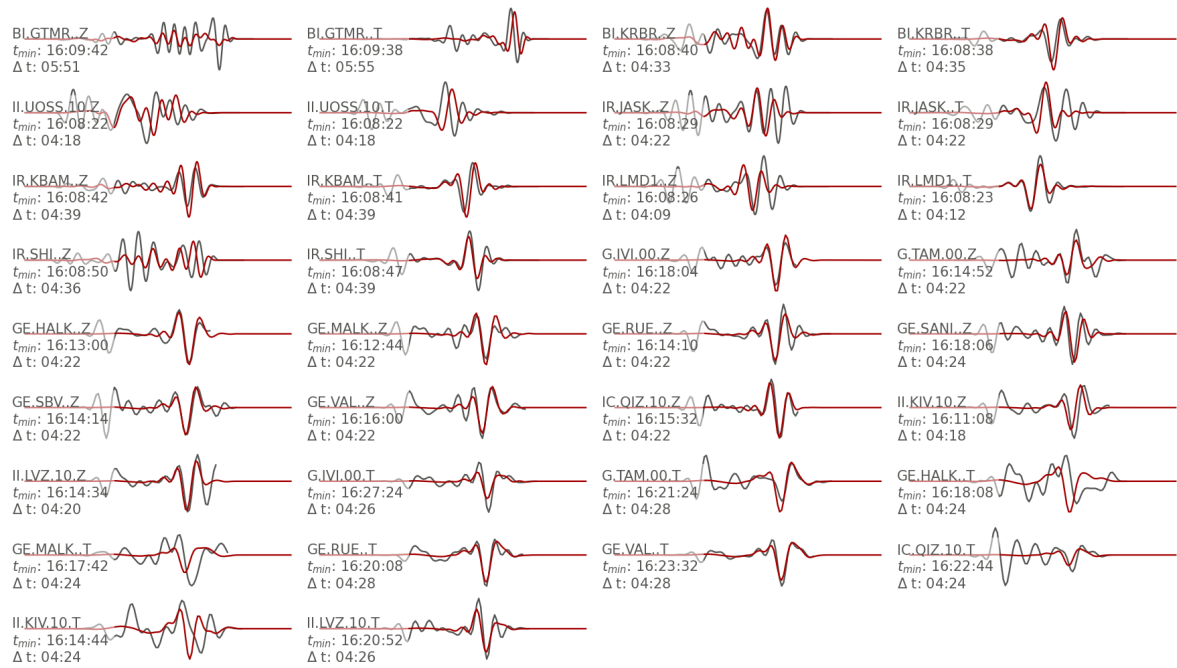


**Figure S5.** Waveform fits of the mean model (red) and observed data (black) from full MT inversion of earthquake B2. Channel information, start time of each trace and length of the given traces are given left of each trace.

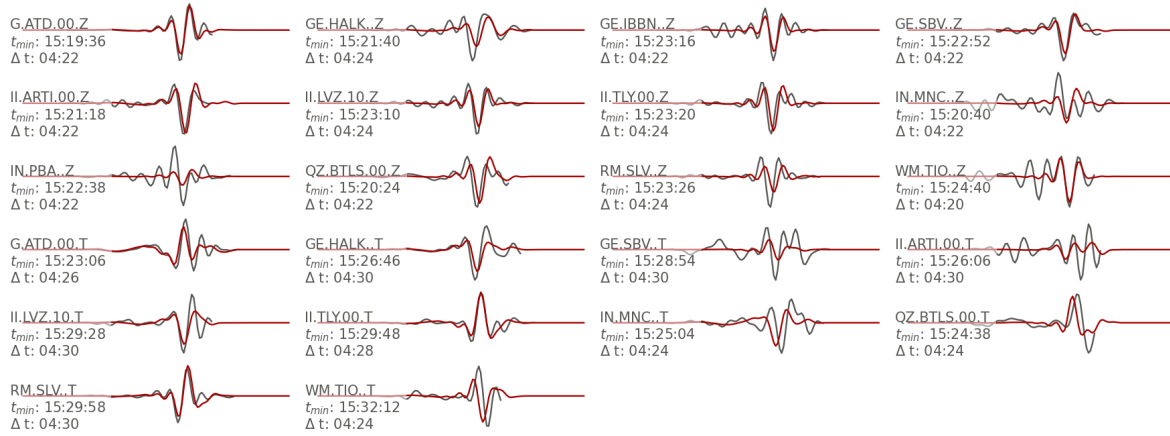


**Figure S6.** Waveform fits of the mean model (red) and observed data (black) from full MT inversion of earthquake C1. Channel information, start time of each trace and length of the given traces are given left of each trace.

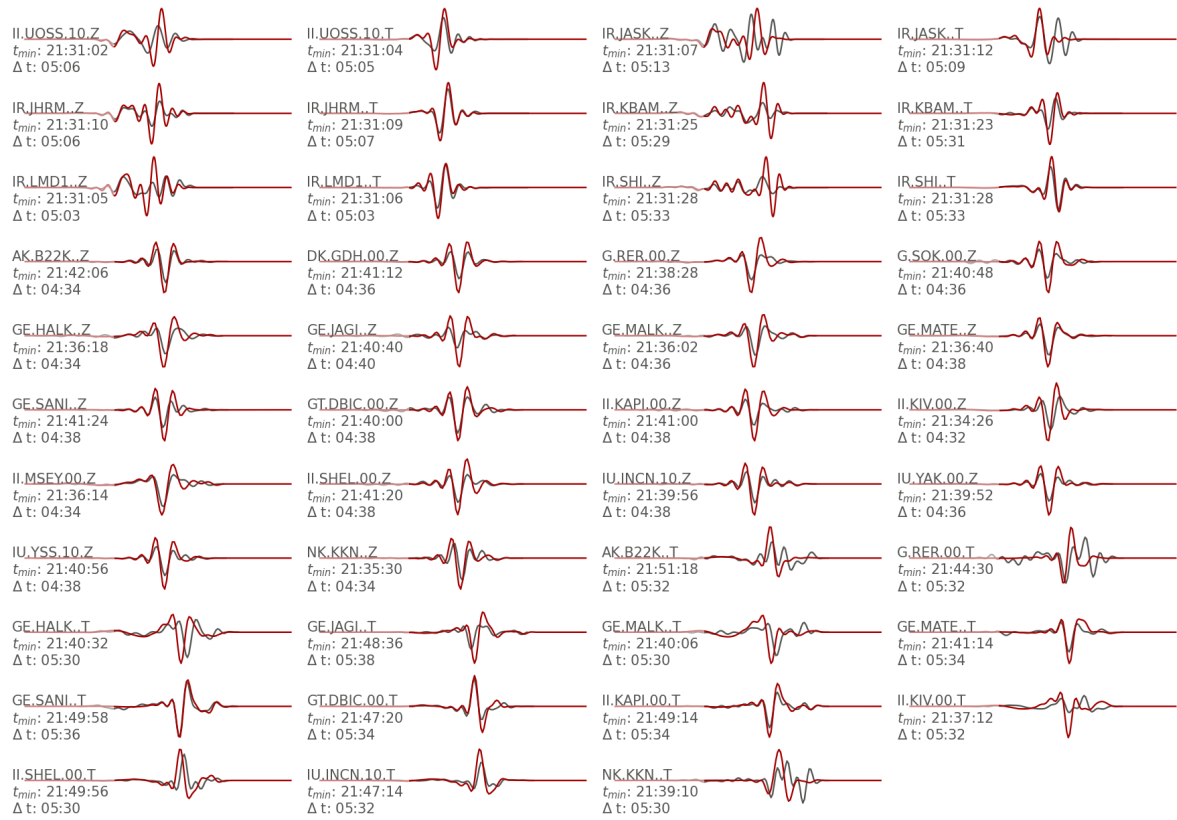


**Figure S7.** Waveform fits of the mean model (red) and observed data (black) from PDR inversion of earthquake A1. Channel information, start time of each trace and length of the given traces are given left of each trace.

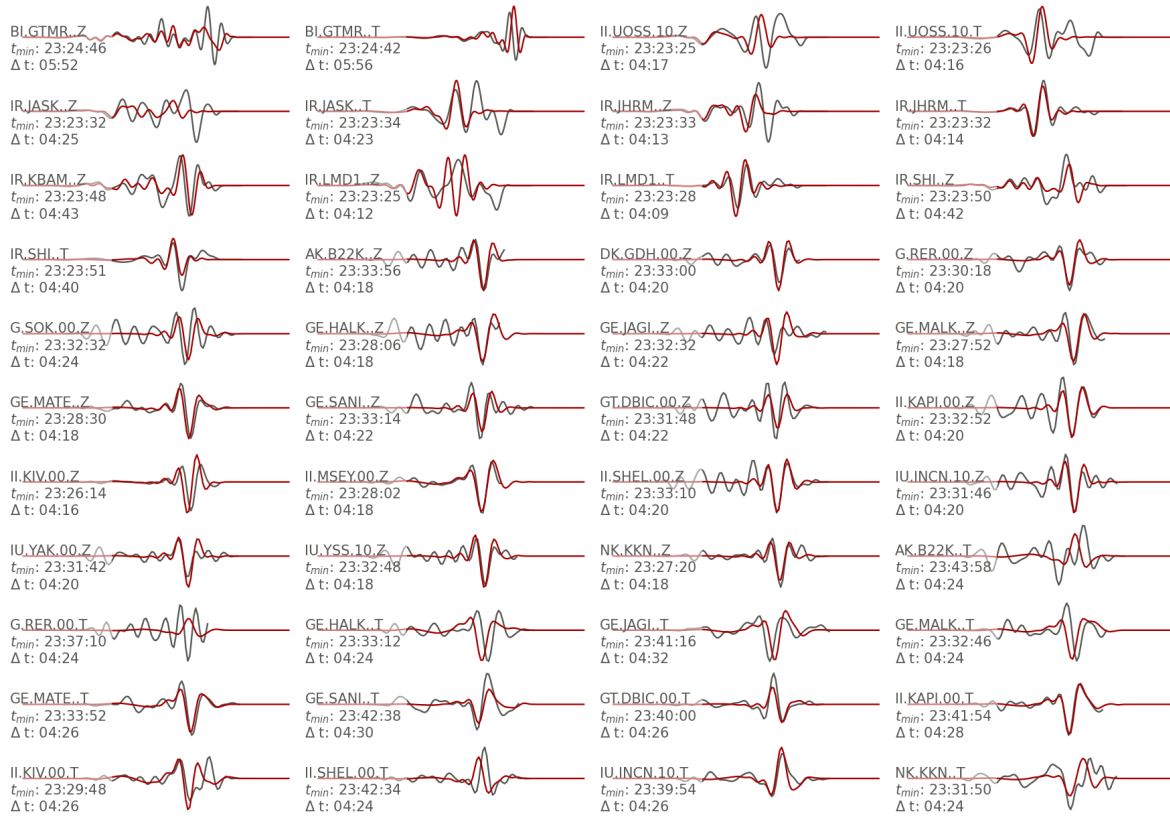


**Figure S8.** Waveform fits of the mean model (red) and observed data (black) from PDR inversion of earthquake A2. Channel information, start time of each trace and length of the given traces are given left of each trace.

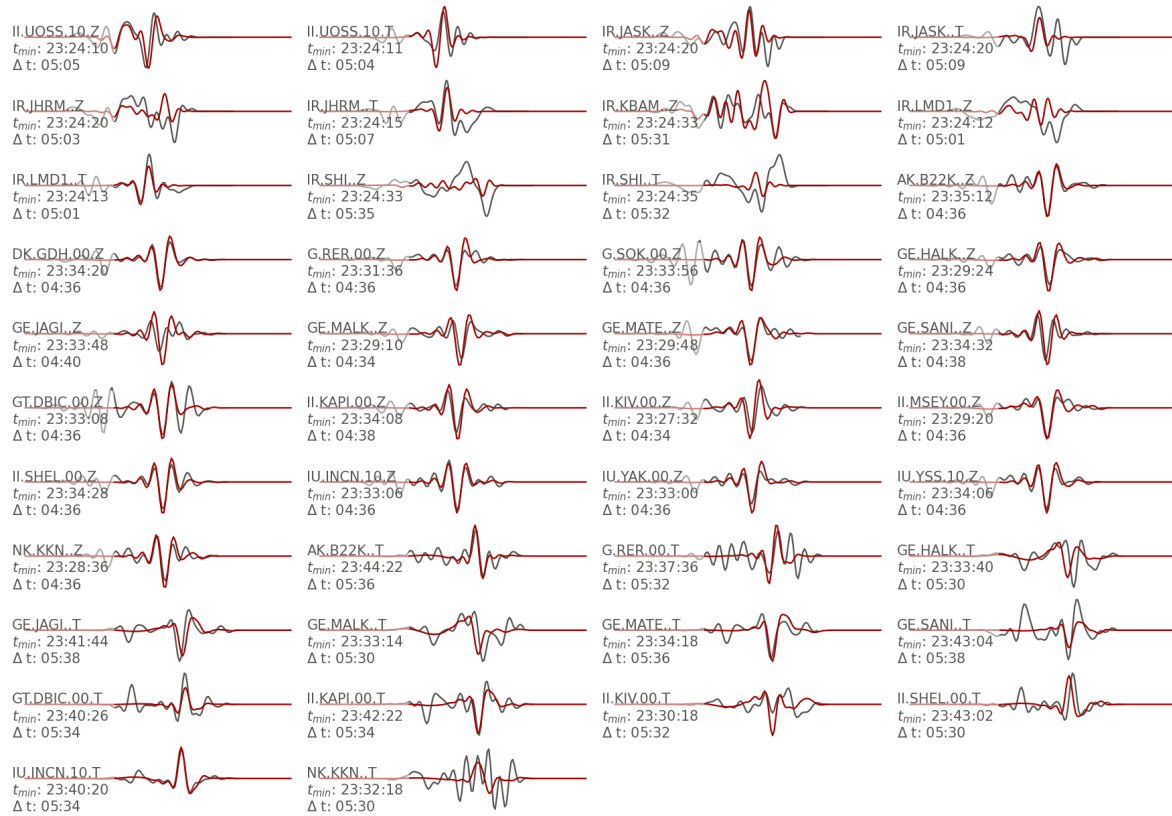


**Figure S9.** Waveform fits of the mean model (red) and observed data (black) from PDR inversion of earthquake A3. Channel information, start time of each trace and length of the given traces are given left of each trace.



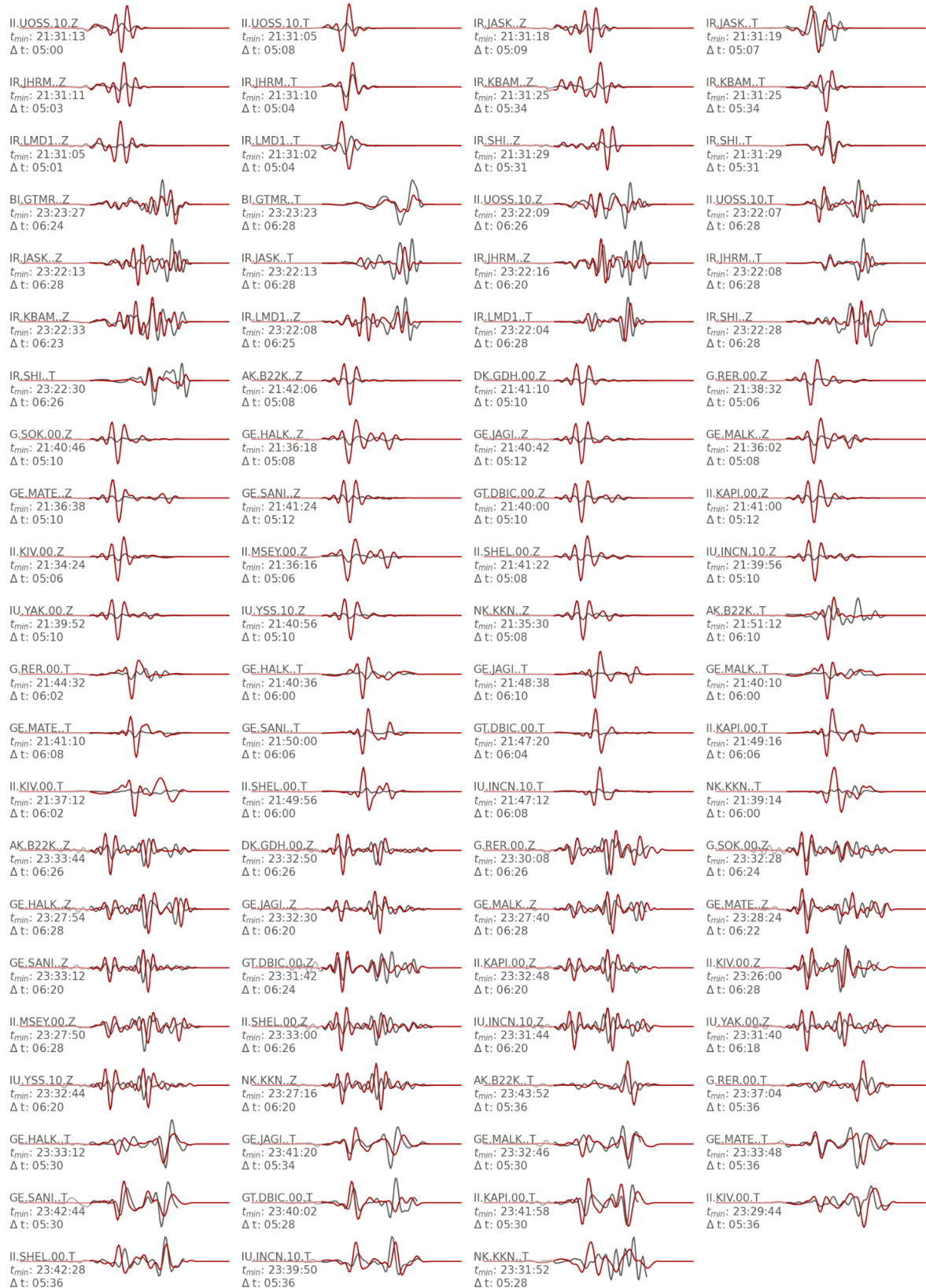


**Figure S11.** Waveform fits of the mean model (red) and observed data (black) from joint 3 PDR inversion of earthquakes A1, A2 and A3 using seismic and satellite deformation data. Channel information, start time of each trace and length of the given traces are given left of each trace.

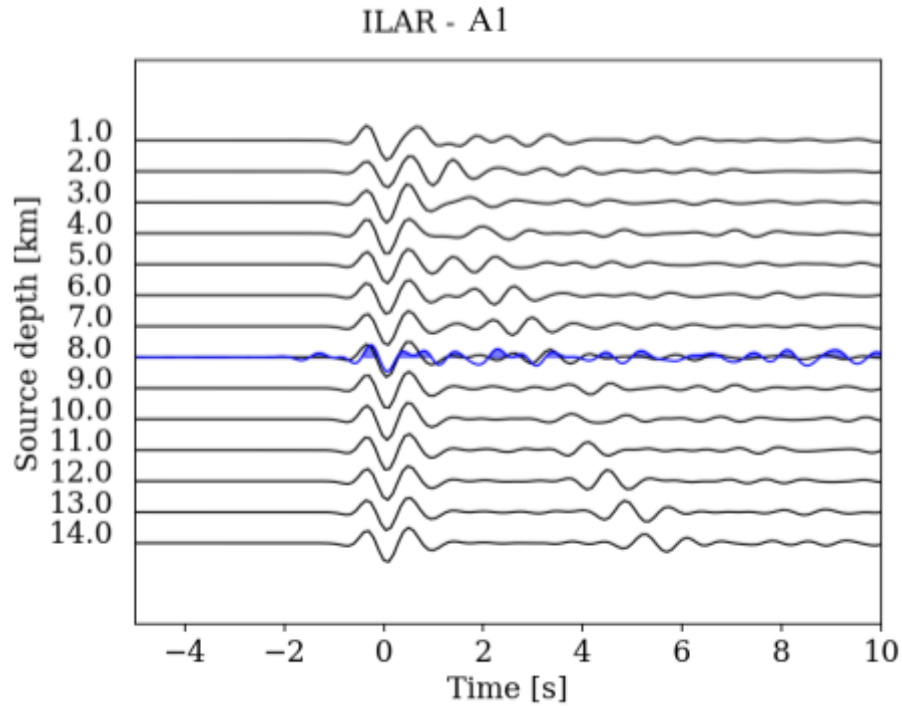


**Figure S12.** Best focal depth estimate for A1 derived from the stacked vertical trace of the ILAR network. Black lines show synthetic traces modelled for a source in the given depths along a path to the array centre. The blue line, shown at the preferred focal point depth, indicates the observed stacked trace of the network.

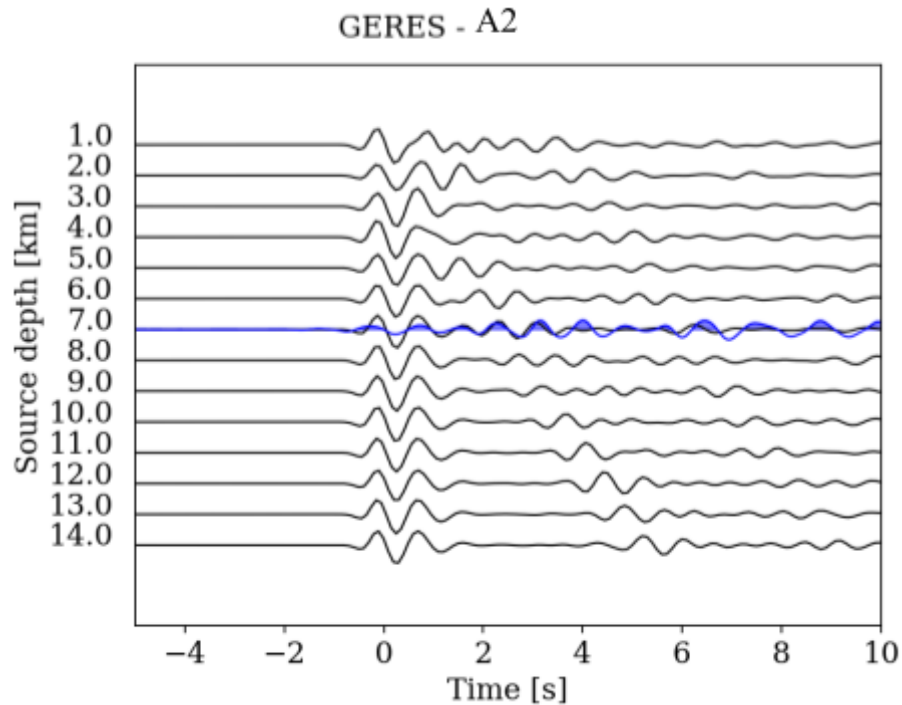


**Figure S13.** Best focal depth estimate for A2 derived from the stacked vertical trace of the GERES network. Black lines show synthetic traces modelled for a source in the given depths along a path to the array centre. The blue line, shown at the preferred focal point depth, indicates the observed stacked trace of the network.

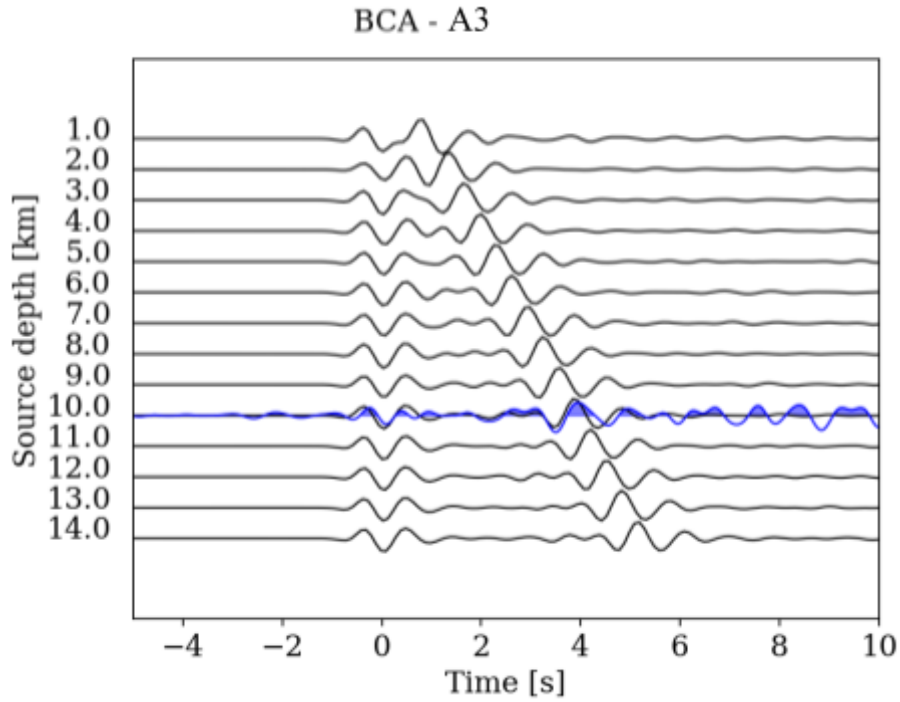


**Figure S14.** Best focal depth estimate for A3 derived from the stacked vertical trace of the BCA network. Black lines show synthetic traces modelled for a source in the given depths along a path to the array centre. The blue line, shown at the preferred focal point depth, indicates the observed stacked trace of the network.

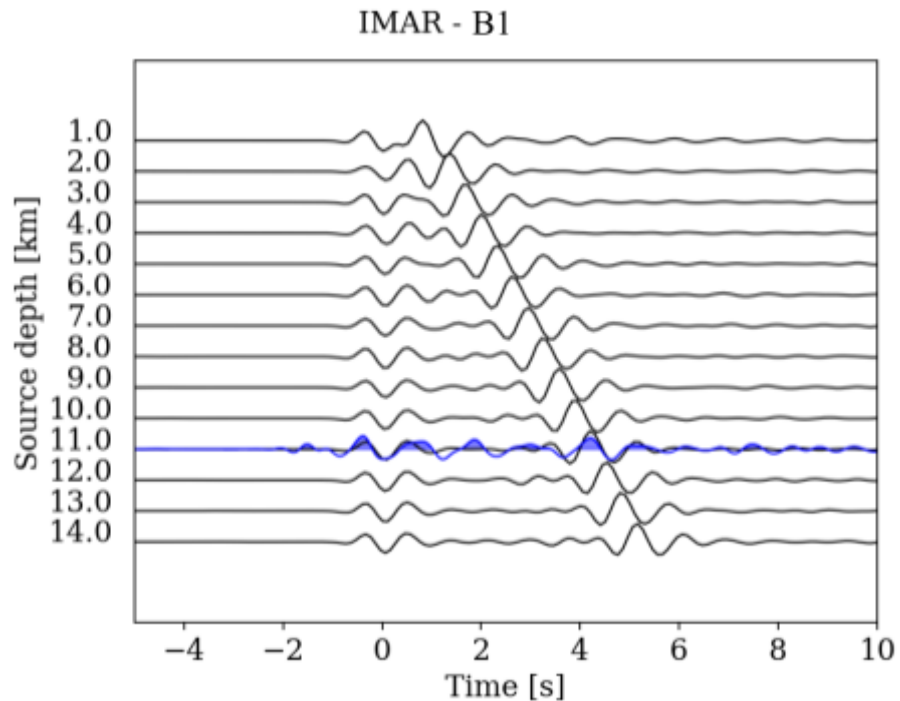


**Figure S15.** Best focal depth estimate for B1 derived from the stacked vertical trace of the IMAR network. Black lines show synthetic traces modelled for a source in the given depths along a path to the array centre. The blue line, shown at the preferred focal point depth, indicates the observed stacked trace of the network.

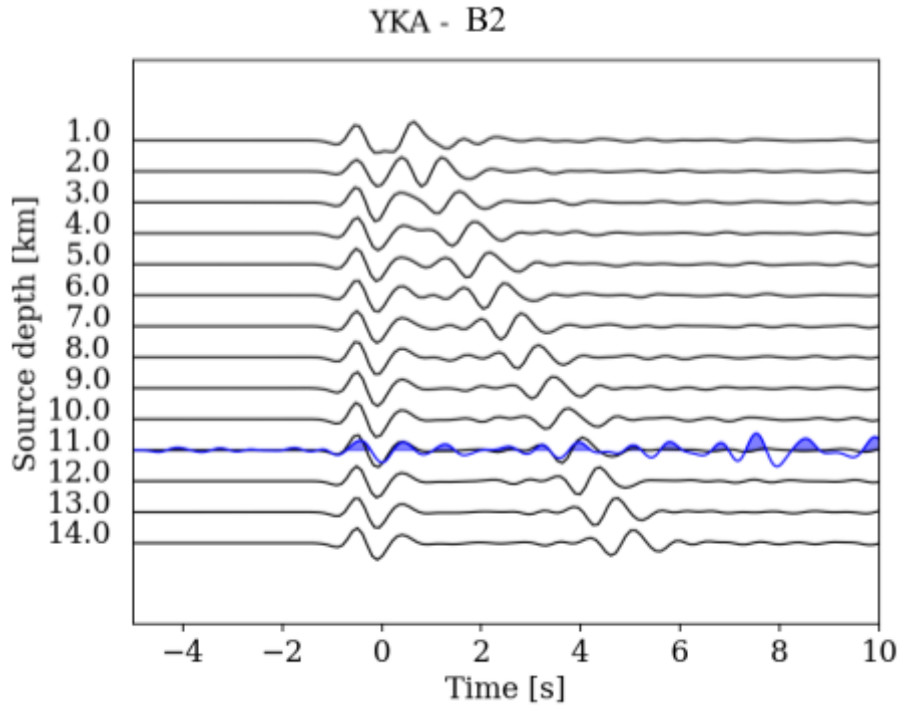


**Figure S16.** Best focal depth estimate for B2 derived from the stacked vertical trace of the YKA network. Black lines show synthetic traces modelled for a source in the given depths along a path to the array centre. The blue line, shown at the preferred focal point depth, indicates the observed stacked trace of the network.

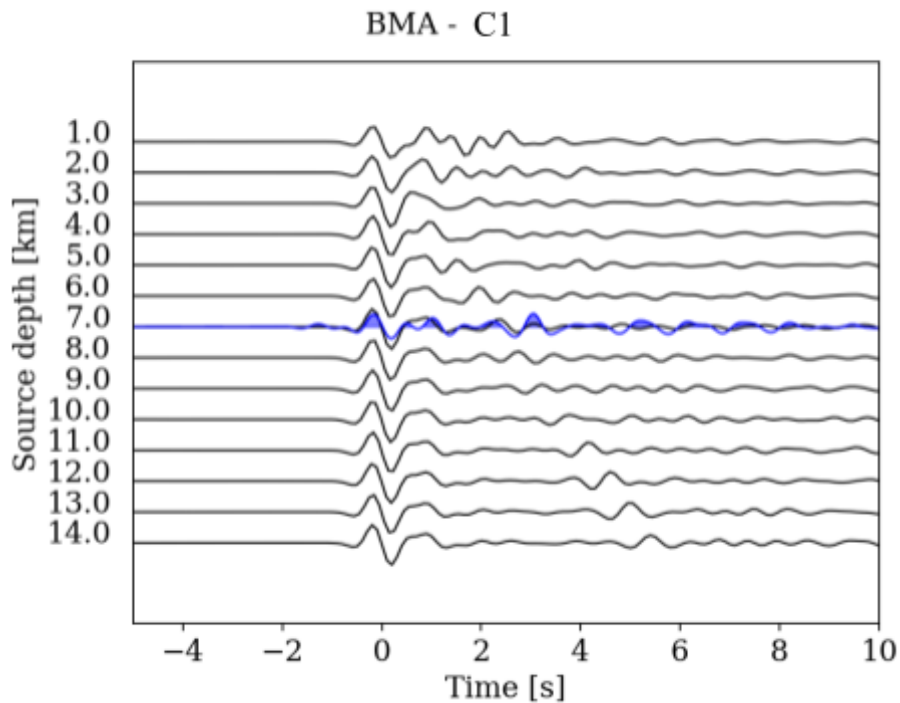


**Figure S17.** Best focal depth estimate for C1 derived from the stacked vertical trace of the BMA network. Black lines show synthetic traces modelled for a source in the given depths along a path to the array centre. The blue line, shown at the preferred focal point depth, indicates the observed stacked trace of the network.

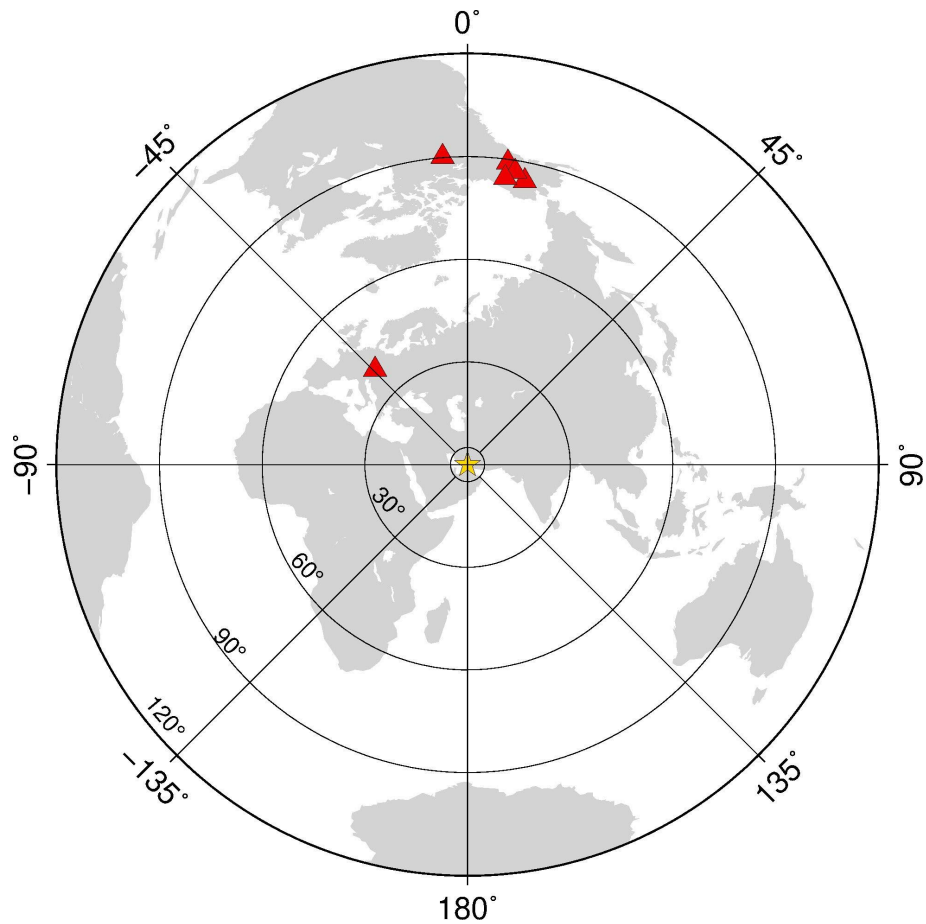


**Figure S18.** Network locations (red triangles) used within the abedeto focal depth estimation tool are shown with respect to the earthquake locations (yellow star). Further information on the networks is given in Table S6.

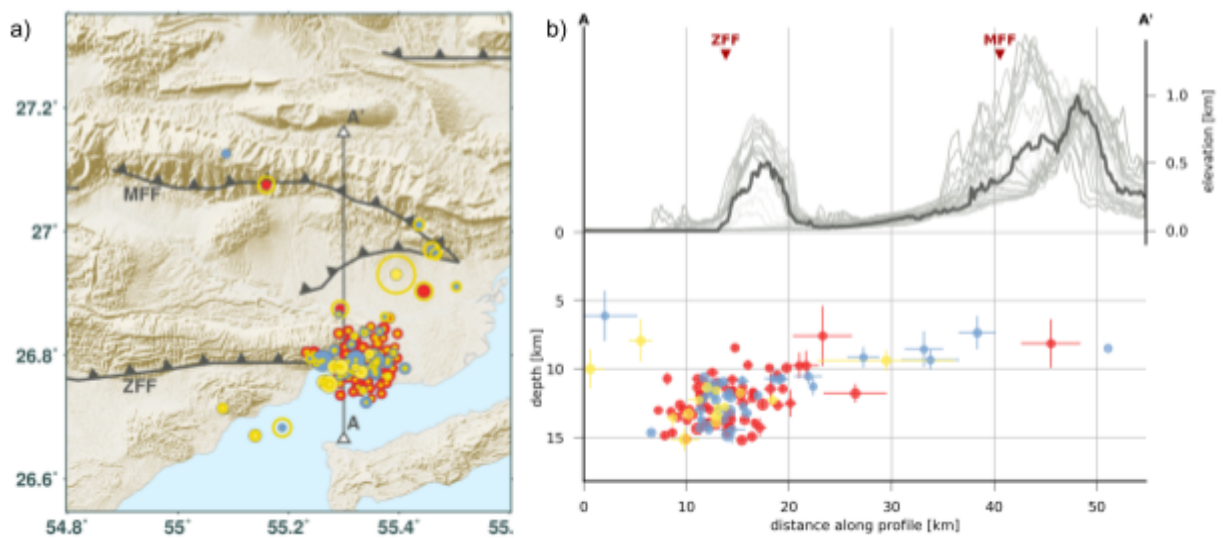


**Figure S19.** Relocated aftershock distribution (a) on map view and (b) along the profile shown in (a). Horizontal location uncertainties in (a) are indicated by yellow circles. Horizontal and vertical location uncertainties in (b) are shown as horizontal and vertical bars.

**Table S1:** Deviatoric moment tensor solutions for the mainshocks derived from seismic data inversion. Standard deviations are given in the same units as values if not denoted separately. Standard deviation values are indicated by *\_std* as part of their parameter name. *rmij* indicates relative moment tensor components. Absolute moment contributions can be derived from them combined with the magnitude.

**Table S2:** Full moment tensor solutions for the mainshocks derived from seismic data inversion. Standard deviations are given in the same units as values if not denoted separately. Standard deviation values are indicated by *\_std* as part of their parameter name. *rmij* indicates relative moment tensor components. Absolute moment contributions can be derived from them combined with the magnitude.

Event ID	A1	A2	A3
date	2022-07-01	2022-07-01	2022-07-01
time	21:32:06.27	23:24:15.71	23:25:15.51
time_std [s]	6.2	2.6	4.4
lat [deg]	26.8345	26.8262	26.8582
north_shift_std [km]	0.3	4.1	0.2
lon [deg]	55.3401	55.1525	55.2701
east_shift_std [km]	0.38	5.1	0.29
strike [deg]	93.9	85	92
strike_std	4.4	19	3.8
dip [deg]	66.1	65	77.6
dip_std	2.7	11	1.6
rake [deg]	79.2	94	94.8
rake_std	7.1	22	4.6
depth [km]	8.27	11.9	6.13
depth_std	0.17	2.7	0.19
mw	6.27	5.78	5.928
mw_std	0.018	0.11	0.028
misfit	0.5446307		

**Table S3:** Double couple (DC) moment tensor solutions for the mainshocks of sequence A derived from a joint 3 DC source inversion using seismic and satellite deformation data. Standard deviations are given in the same units as values if not denoted separately. Standard deviation values are indicated by *\_std* as part of their parameter name. *rmij* indicates relative moment tensor components. Absolute moment contributions can be derived from them combined with the magnitude.

**Table S4:** PDR finite fault solutions for the mainshocks derived from seismic data inversions. Less preferred solutions inverting for the auxiliary nodal planes are shown in dark grey columns. Standard deviations are given in the same units as values if not denoted separately. Standard deviation values are indicated by *\_std* as part of their parameter name. *Gamma* indicates the ratio between rupture and shear wave velocity. *Depth* refers to the depth of the top edge of the resolved rupture plane. The location given with *Lat* and *Lon* resolves the top edge centre location.

**Table S5:** PDR finite fault solutions for the mainshocks derived from a joint 3 PDR inversion using seismic and satellite deformation data. Standard deviations are given in the same units as values if not denoted separately. Standard deviation values are indicated by *\_std* as part of their parameter name. *Gamma* indicates the ratio between rupture and shear wave velocity. *Depth* refers to the depth of the top edge of the resolved rupture plane. The location given with *Lat* and *Lon* resolves the top edge centre location.

Event ID	ArrayCode	Array Center Lat [deg]	Array Center Lon [deg]	Focal depth [km]
A1	ILAR	64.77045	-146.87907	8.0
A2	GERES	48.83591	13.70060	8.0
A3	BCA	63.06266	-141.78724	10.0
B1	IMAR	65.98615	-153.75525	11.0
B2	YKA	62.49937	-114.67831	11.0
C1	BMA	67.42937	-144.55291	7.0

**Table S6:** Information on used arrays and retrieved focal depth for the six mainshocks using the abedeto tool. Array codes and centre coordinates are given.